Nuclear Suppression in Diffractive Vector Meson Production

Research training

Heikki Mäntysaari

August 25, 2011

University of Jyväskylä
Department of Physics

Supervisor: Tuomas Lappi

Abstract

In this research training report diffractive electron-proton and electron-nucleus scattering processes are studied using the so called dipole model. In the dipole picture this process is described as the incoming electron emitting a virtual photon which fluctuates into a quark-antiquark dipole. This dipole then scatters elastically off the hadron and forms the final state particles, e.g. a J/Ψ vector meson. Diffraction means here that there is no exchange of quantum numbers between the virtual photon and the hadron.

It is shown that the individual nucleons inside the nucleus cannot be resolved at high energy even at reasonably large virtualities of the exchanged virtual photon. Instead, there is a strong nuclear suppression due to the saturation effects. Strong suppression is expected as the incoherent cross section is proportional to the nucleus mass number A in the dilute limit and to $A^{1/3}$ in the black disk limit.

Tiivistelmä

Tässä erikoistyössä tarkastellaan diffraktiivista elektroni–protoni- ja elektroni–ydinsirontaa ja sen kuvaamista dipolimallilla. Dipolikuvassa prosessi tapahtuu siten, että leptoni emittoi virtuaalisen fotonin, joka fluktuoituu kvarkki–antikvarkkidipoliksi. Syntynyt dipoli siroaa hadronista elastisesti ja muodostaa tämän jälkeen lopputilan hiukkaset, esimerkiksi J/Ψ-vektorimesonin. Diffraktiolla tarkoitetaan tässä yhteydessä sitä, että virtuaalisen fotonin ja hadronin välillä ei vaihdeta kvanttilukuja.

Tutkimuksen tuloksena haviataan, että ytimen sisällä olevia nukleoneja ei voida erottaa toisistaan suurienergisissä sirontaprosesseissa edes silloin, kun vaihdettavalla fotonilla on suuri virtualiteetti. Analyyttiset ja numeeriset laskut antavat voimakkaan ydinsuppression joka johtuu saturaatioilmiöistä. Voimakas suppressio on odotettavissa, sillä epäkoherentti vaikutusala on verrannollinen ytimen massalukuun A suuren virtualiteetin rajalla ja $A^{1/3}$:een rajalla, jossa dipoli aina siroaa ytimestä.

List of publications

[1] T. Lappi and H. Mäntysaari, "Incoherent diffractive J/Ψ production in high-energy nuclear deep-inelastic scattering". *Phys. Rev.* **C83** (2011) 065202, arXiv:1011.1988 [hep-ph].

The author has derived the formulae for incoherent dipole-nucleus scattering discussed in [1]. He also wrote the numerical code to compute the cross sections and participated in the interpretation of the results.

Contents

1 Introduction

In particle physics the elementary matter particles and their interactions, excluding gravity, are described by the Standard Model. It describes three kind of interactions: electromagnetic, weak and strong. Moreover, electromagnetic and weak interactions are described as two aspects of the same force, namely the electroweak interaction. All particles interact via the electroweak interaction. The third interaction in the Standard Model is the strong interaction described by the quantum chromodynamics (QCD). Quarks and gluons, the particles that e.g. a proton consists of, also interact via the strong interaction.

Today QCD is an accurately tested part of the Standard Model, but not all about strong interactions is known. QCD is a so called non-Abelian gauge theory which makes it difficult to investigate. For example the properties of the quark-gluon plasma (QGP), the state of matter that can be produced in ultra relativistic heavy ion collisions at high energy, are not known in detail.

In this work the phenomenology of electron-proton and electron-nucleus collisions at high energy is studied. These studies allow us to determine the initial conditions of the heavy ion collisions, e.g. the gluon distributions inside the nucleus. The proposed future electron-ion colliders, such as eRHIC at Brookhaven [2] and LHeC at CERN [3], can investigate these properties.

1.1 Outline

The goal of this report is to study virtual photon-nucleus collisions, a subprocess of the complete electron-nucleus scattering. We are mainly interested in how the saturation effects affect the cross section compared with the scattering off independent protons. We characterize nuclear effects by the ratio of virtual photon-nucleus cross section to the virtual photon-proton cross section normalized by the number of nucleons. In this work we refer to this quantity as the *nuclear suppression*.

In the first chapter we introduce some terminology and study the kinematics of the scattering events we are interested in. In chapter 2 we introduce the dipole model to describe virtual photon-nucleus collision at high energy. In chapter 3 we analyze the nuclear suppression in detail.

1.2 Notation

Vectors are written as a plain letters without any vector sign, e.g. p for the 4-momentum. Operators and matrices are written in capital letters, e.g. S for the scattering matrix.

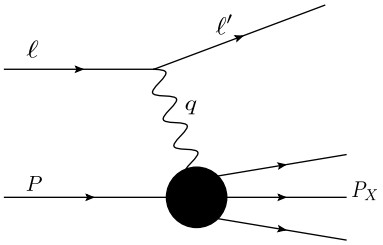

Figure 1. Deep inealstic scattering.

The system of units in which $\hbar = c = k_B = 1$ is used. In this case the fine-structure constant $\alpha_{\text{em}} = e^2/(4\pi) \approx 137^{-1}$, where e is the elementary charge. In this system of units

$$[\text{mass}] = [\text{energy}] = [\text{time}]^{-1} = [\text{length}]^{-1} = \text{GeV}. \tag{1.1}$$

In some cases the relation between gigaelectronvolts and femtometers is needed:

$$1 \text{ GeV} = 5.0677 \text{ fm}^{-1}. \tag{1.2}$$

1.3 Deep inelastic scattering

Deep inelastic scattering (DIS) is a powerful way to measure the internal structure of hadrons and to test perturbative QCD. In DIS a lepton scatters off a hadron which then breaks up into other particles making the process inelastic. Let us consider deep inelastic scattering of the lepton l off the nucleus N. In this case we can write the process as

$$l(\ell) + N(P) \to l'(\ell') + X(P_X), \tag{1.3}$$

where P is the momentum of the incoming nucleus and ℓ and ℓ' are the momenta of the incoming and outgoing lepton, respectively. In this process the nucleus breaks up and forms many different particles which are denoted by X with momentum P_X. The situation is shown schematically in Fig. 1.

To describe the kinematics of the deep inelastic scattering we define the following Lorentz invariant variables:

$$q^2 \equiv -Q^2 \equiv (\ell - \ell')^2 \tag{1.4}$$

$$\nu \equiv \frac{P \cdot q}{m_A} = \frac{W^2 + Q^2 - m_A^2}{2m_A} \tag{1.5}$$

$$x \equiv \frac{AQ^2}{2P \cdot q} = \frac{AQ^2}{2m_A \nu} = \frac{AQ^2}{Q^2 + W^2 - m_A^2}. \tag{1.6}$$

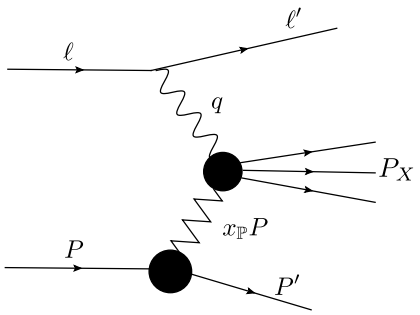

Figure 2. Diffractive deep inelastic scattering. Pomeron is represented by a zigzag line.

Here $W^2 = (P+q)^2$ is the Mandelstam s variable for the photon-nucleus scattering, m_A is the mass of the nucleus and A is the mass number of the nucleus. ν describes the total energy transferred in the process in the target rest frame: $\nu = E_l - E_l'$ where E_l and E_l' are lepton energies at the beginning and at the end of the process in the proton rest frame, respectively. The variable x is called Bjorken x and it is the fraction of average nucleon momentum (in the infinite momentum frame where the momentum of the nucleus is very large) carried by the quark or the gluon taking part in the scattering process.

1.4 Diffractive deep inelastic scattering

Diffractive deep inelastic scattering (DDIS) means a DIS process in which there is no exchange of quantum numbers between the virtual photon and the hadron [4]. One can describe such a process by saying that an object, which carries the quantum numbers of the vacuum, is exchanged between the virtual photon and the hadron. Such a particle is called *pomeron*. After the pomeron exchange the virtual photon hadronizes and forms the outgoing particles X with momentum P_X shown in Fig. 2.

However the pomeron is not a real observable particle but just a model used to describe this process. What we really see experimentally in e.g. diffractive ep scattering is a large rapidity gap between X and the outgoing proton, as the pomeron has carried momentum but not color charge. If the process was not diffractive, then there would be a transfer of color charge and thus the color string between outgoing p and X would generate a parton cascade which would fill the whole rapidity space.

In addition to the kinematical variables defined in Sec. 1.3 we define the

following variables in order to describe DDIS kinematics:

$$t \equiv -(P' - P)^2 \tag{1.7}$$

$$x_{\mathbb{P}} \equiv \frac{A(P - P') \cdot q}{P \cdot q} = A\frac{M^2 + Q^2 - t}{W^2 + Q^2 - m_A^2} \approx A\frac{M^2 + Q^2}{W^2 + Q^2}. \tag{1.8}$$

Here M^2 is the invariant mass squared of the system of particles denoted by X. The interpretation of $x_{\mathbb{P}}$ is that it gives the fraction of the average nucleon momentum carried by the pomeron in the infinite momentum frame. The Mandelstam variable t describes the momentum transfer between the nucleus and the photon. It is also useful to notice the relation between the Bjorken x defined in Eq. (1.6) and $x_{\mathbb{P}}$:

$$x_{\mathbb{P}} \approx x\left(1 + \frac{M^2}{W^2}\right). \tag{1.9}$$

1.5 Scattering matrix and the optical theorem

Let us consider a scattering process in which the system evolves from state $|i\rangle$ to state $|f\rangle$, and the evolution is described by the operator S:

$$|f\rangle = S|i\rangle. \tag{1.10}$$

This scattering matrix (S matrix) can be used to describe the physics of the scattering process. As it is also possible that the initial and the final states are the same, it is convenient to define operator T such that

$$S = \mathbb{1} + iT. \tag{1.11}$$

From this we see that the diagonal elements of the S matrix give the probability amplitude that the particle does not scatter off the target. The T matrix gives the scattering amplitude: $T_{ij} = i\mathcal{A}(i \to j)$. Conservation of probability requires that S is a unitary matrix:

$$1 = \sum_f |\langle f|S|i\rangle| = \sum_f \langle i|S|f\rangle\langle f|S^\dagger|i\rangle = \langle i|SS^\dagger|i\rangle, \tag{1.12}$$

so $SS^\dagger = \mathbb{1}$ as the state i is arbitrary.

Requiring that $SS^\dagger = \mathbb{1}$ and substituting $S = \mathbb{1} + iT$ one can derive the *optical theorem*, namely that [4]

$$\sigma_{\text{tot}} = 2\,\text{Im}\,\mathcal{A}_{\text{el}}(t = 0). \tag{1.13}$$

This means that the total cross section can be obtained directly from the imaginary part of the forward elastic scattering amplitude.

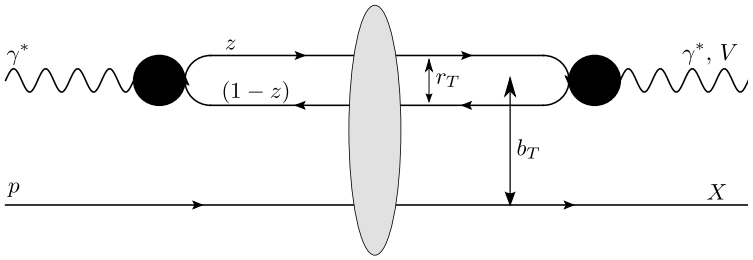

Figure 3. $\gamma^* p$ scattering in the dipole picture.

2 Dipole model

In the dipole model diffractive deep inelastic electron-proton or electron-nucleus scattering (at small x) is described as follows: first an incoming electron emits a virtual photon, which then fluctuates into a quark-antiquark ($q\bar{q}$) color dipole. This dipole then scatters elastically off the target and recombines to form the final state particles, e.g. a virtual photon or a meson [5]. This process is shown schematically in Fig. 3.

2.1 Derivation of the dipole model

We can see that this model, in which the virtual photon fluctuates into a quark-antiquark dipole, works if the lifetime of the dipole is long compared to the characteristic time scale of the scattering event. The following discussion follows the one in Ref. [4].

Consider the $\gamma^* p$ scattering in the proton rest frame (the same derivation works also with the $\gamma^* A$ scattering). Using the kinematical variables defined in Sec. 1.3 we can write the virtual photon momentum as $p_{\gamma^*} = (\nu, 0, 0, \sqrt{\nu^2 + Q^2})$. In the light cone coordinates this reads [1]

$$p_{\gamma^*} = \left(q^+, -\frac{Q^2}{2q^+}, 0 \right), \tag{2.1}$$

where, at small x, $q^+ \approx \sqrt{2}\nu$.

Let us then consider the produced quarks with momenta κ for the quark and κ' for the antiquark. If we denote the transverse momentum of the quark by κ_T and require that the produced (approximately massless) quarks are on

[1] In the light-cone coordinates the vector (A^0, A^1, A^2, A^3) is written as (A^+, A^-, A_T), where $A^\pm = \frac{1}{\sqrt{2}}(A^0 \pm A^3)$ and $A_T = (A^1, A^2)$. The inner product is $A \cdot B = A^+ B^- + A^- B^+ - A_T \cdot B_T$.

mass shell we get, again in light-cone coordinates,

$$\kappa = \left(zq^+, \frac{\kappa_T^2}{2zq^+}, \kappa_T \right), \text{ and} \tag{2.2}$$

$$\kappa' = \left((1-z)q^+, \frac{\kappa_T^2}{2(1-z)q^+}, -\kappa_T \right). \tag{2.3}$$

Here z is the fraction of the light cone momentum of the photon carried by the quark. The invariant mass squared of the pair is

$$M^2 = (\kappa + \kappa')^2 = \frac{\kappa_T^2}{z(1-z)}. \tag{2.4}$$

Now the formation time of the dipole is $\tau \sim 1/\Delta E$, where ΔE is the energy difference between the virtual photon and the dipole. In light-cone coordinates the energy of the quark can be obtained as $E_\kappa = \frac{1}{\sqrt{2}}(\kappa^+ + \kappa^-)$. Thus

$$\Delta E = E_{\text{dipole}} - E_{\gamma^*} = E_\kappa + E_{\kappa'} - E_{\gamma^*} = \frac{1}{2\sqrt{2}q^+} \left(Q^2 + \frac{\kappa_T^2}{z(1-z)} \right). \tag{2.5}$$

From Eq. (2.4) we see that $\kappa_T^2 = z(1-z)M^2$. We can also assume that M^2 and Q^2 are approximately the same, which allows us to approximate

$$\Delta E \approx \frac{Q^2}{\sqrt{2}q^+} \approx \frac{Q^2}{2\nu} = m_N x. \tag{2.6}$$

Here m_N is the mass of the target proton, see Sec. 1.3. Thus $\tau \sim 1/(m_N x)$. On the other hand the interaction time $\tau_{\text{int}} \sim R_p$, where R_p is the proton radius, which is constant and thus much smaller than τ at small x. This also gives us the reason to approximate that the size of the dipole is constant during the interaction.

2.2 Dipole-proton scattering

Let's first consider diffractive $\gamma^* p \to Vp$ scattering, where we denote by V the produced final state particle, for example a J/Ψ vector meson. Using the kinematical variables defined in Secs. 1.3 and 1.4 we can write the scattering amplitude as

$$\mathcal{A}_{T,L}^{\gamma^* p \to Vp}(x, Q, \Delta_T) = \int \mathrm{d}^2 r_T \int_0^1 \frac{\mathrm{d}z}{4\pi} [\Psi_V^* \Psi]_{T,L}(r_T, z, Q) \mathcal{A}_{q\bar{q}}(x, r_T, \Delta_T). \tag{2.7}$$

Here $\mathcal{A}_{q\bar{q}}(x, r, \Delta)$ is the scattering amplitude for a dipole of transverse size r_T to scatter off the proton and Δ_T is the transverse momentum lost by the outgoing proton. The fraction of the virtual photon momentum carried by the quark is z, see Fig. 3. For simplicity we have dropped the helicity indexes from the virtual photon wave function. In case of deeply virtual Compton scattering, where the produced final state particle is a real photon, the amplitude must be summed over all possible quark flavors.

The probability amplitude for the virtual photon to fluctuate into $q\bar{q}$ dipole is Ψ, and similarly Ψ_V^* is the probability amplitude for the $q\bar{q}$ to fluctuate into the final state V. We discuss about these functions in more detail in Sec. 2.3. In this notation the differential cross section is

$$\frac{\mathrm{d}\sigma_{\gamma^* p}}{\mathrm{d}t} = \sum_{T,L} \frac{1}{16\pi} |\mathcal{A}_{T,L}^{\gamma^* p}(x, Q, \Delta_T)|^2. \tag{2.8}$$

The summation is taken over the polarization states of the virtual photon.

To get $\mathcal{A}_{q\bar{q}}(x, r_T, \Delta)$ we use the fact that the color dipole scatters elastically off the hadron, and thus we can use the optical theorem introduced in Sec. 1.5. First we notice that Δ_T is the Fourier conjugate of the impact parameter b_T [2], so

$$\begin{aligned} \mathcal{A}_{q\bar{q}}(x, r_T, \Delta_T) &= \int \mathrm{d}^2 b_T e^{-i b_T \cdot \Delta_T} \mathcal{A}_{q\bar{q}}(x, r_T, b_T) \\ &= i \int \mathrm{d}^2 b_T e^{-i b_T \cdot \Delta_T} 2[1 - S(x, r_T, b_T)], \end{aligned} \tag{2.9}$$

where $S = 1 - iT$ is the scattering matrix of the $q\bar{q}p$ scattering process. The optical theorem, Eq. (2.9), then leads us to the expression

$$\sigma_{q\bar{q}}^{\mathrm{tot}} = 2 \,\mathrm{Im}\, \mathcal{A}_{q\bar{q}}(x, r, \Delta_T = 0) = \int \mathrm{d}^2 b_T 2[1 - \mathrm{Re}\, S(x, r_T, b_T)]. \tag{2.10}$$

Thus we can define

$$\frac{\mathrm{d}\sigma_{q\bar{q}}}{\mathrm{d}^2 b_T} = 2[1 - \mathrm{Re}\, S(x, r_T, b_T)] \approx 2[1 - S(x, r, b_T)], \tag{2.11}$$

where we assumed that the S matrix is completely real. This causes an error of the order of 10% to the squared amplitude which must be taken into account when comparing results with the experimental data. The required corrections are described in Sec. 2.6. Comparing Eqs. (2.11) and (2.9) one can write

$$\mathcal{A}_{q\bar{q}}(x, r_T, \Delta_T) = i \int \mathrm{d}^2 b_T e^{-i b_T \cdot \Delta_T} \frac{\mathrm{d}\sigma_{q\bar{q}}}{\mathrm{d}^2 b_T}. \tag{2.12}$$

[2] The Fourier conjugate of b_T is Δ_T only if the dipole is small, see discussion in Sec. 2.7.

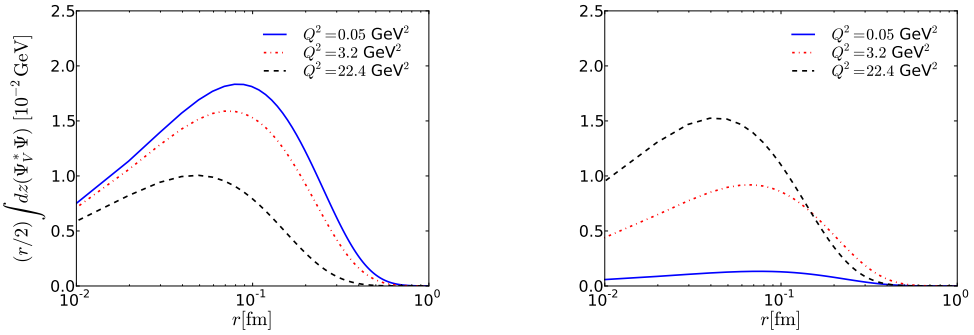

(a) Transverse polarization **(b)** Longitudinal polarization

Figure 4. Overlap between the virual photon and the J/Ψ meson wave functions in the boosted Gaussian parametrization [5].

Notice that elastic dipole-proton cross section is now

$$\frac{\mathrm{d}\sigma_{q\bar{q}}^{\mathrm{el}}}{\mathrm{d}t} = \frac{1}{16\pi}\left|\mathcal{A}_{q\bar{q}}(x, r_T, t)\right|^2 . \tag{2.13}$$

What is then left is to get the dipole-proton cross section as a function of the impact parameter b_T. There are a few different models available for that quantity, and we consider here the so called IPsat and IIM models. These models are described in detail in Sec. 2.4.

The dipole picture is powerful in a sense that it allows us to calculate (at small x) both the diffractive and total cross sections and the structure function F_2 from the same dipole cross section. This is due to the fact the optical theorem allows us to write F_2 as

$$\begin{aligned} F_2(x, Q^2) &= \frac{Q^2}{4\pi^2\alpha_{\mathrm{em}}}\sigma_{\gamma^* p} = \frac{Q^2}{4\pi^2\alpha_{\mathrm{em}}} 2\,\mathrm{Im}\,\mathcal{A}^{\gamma^* p\to\gamma^* p}(x, Q, \Delta = 0) \\ &= \frac{Q^2}{4\pi^2\alpha_{\mathrm{em}}}\sum_{L,T}\int \mathrm{d}^2 r \int_0^1 \frac{\mathrm{d}z}{4\pi}[\Psi^*\Psi]_{L,T}(r_T, z, Q)\sigma_{q\bar{q}}^{\mathrm{tot}} \end{aligned} \tag{2.14}$$

where the summation is taken over the virtual photon polarization states. If the summation is removed and $\Psi^*\Psi$ is replaced by $[\Psi^*\Psi]_L$ one gets the longitudinal structure function F_L.

2.3 Wave functions

To calculate the scattering amplitude in dipole model we saw that we need the overlap between the photon and the vector meson wave functions, denoted by

$\Psi_V^*\Psi$ in Eq. (2.7). The interpretation of this is that Ψ_V gives the probability amplitude for a particle V to fluctuate into the $q\bar{q}$ dipole, and similarly Ψ is the probability amplitude for a virtual photon to fluctuate into the dipole. There are a few different models available for this product, and in the following discussion we follow Ref. [5].

The function $\Psi^*\Psi$, where the final state is also a virtual photon, can be calculated from the lowest order QED assuming small dipoles, and the result is

$$(\Psi^*\Psi)_T^f = \frac{2N_c}{\pi}\alpha_{em}e_f^2\left\{[z^2+(1-z)^2]+\epsilon^2K_1^2(\epsilon r)+m_f^2K_0^2(\epsilon r)\right\}, \quad (2.15)$$

$$(\Psi^*\Psi)_L^f = \frac{8N_c}{\pi}\alpha_{em}e_f^2Q^2z^2(1-z)^2K_0^2(\epsilon r). \quad (2.16)$$

Here f is the quark flavour, $N_c = 3$ number of colors and $\epsilon^2 = z(1-z)Q^2+m_f^2$. The mass and electric charge of the quark are denoted by m_f and e_f. The functions K_0 and K_1 are modified Bessel functions of the second kind which satisfy $K_{0,1}(x) \sim x^{-1/2}e^{-x}$ at large x, thus the contribution of large dipoles is suppressed by an exponential factor.

Assuming that the vector meson is a quark-antiquark state whose spin and polarization structure is the same as that of a photon, a similar expression can be derived for the overlap between the virtual photon and the vector meson wave functions. As a result one gets the following equations:

$$(\Psi_V^*\Psi)_T = e_f\frac{N_c}{\pi z(1-z)}\left[m_f^2K_0(\epsilon r)\phi_T(r,z)-(z^2+(1-z)^2)\epsilon K_1(\epsilon r)\partial_r\phi_T(r,z)\right] \quad (2.17)$$

$$(\Psi_V^*\Psi)_L = e_f\frac{N_c}{\pi}2Qz(1-z)K_0(\epsilon r)\left[M_V\phi_L(r,z)+\delta\frac{m_f^2-\nabla_r^2}{M_Vz(1-z)}\phi_L(r,z)\right]. \quad (2.18)$$

In so called "Gaus-LC" model the functions ϕ_T and ϕ_L are

$$\phi_T(r,z) = N_T\left[z(1-z)\right]^2e^{-r^2/(2R_T^2)}, \text{ and} \quad (2.19)$$

$$\phi_L(r,z) = N_Lz(1-z)e^{-r^2/(2R_L^2)}. \quad (2.20)$$

Here we also use notation $\nabla_r^2 = (1/r)\partial_r+\partial_r^2$. For the J/Ψ meson the constant factors are [5]: $M_V = 3.097$ GeV, $m_f = 1.4$ GeV, $N_T = 1.23$, $N_L = 0.83$, $R_T^2 = 6.5$ GeV^{-2}, $R_L^2 = 3.0$ GeV and $\delta = 0$.

An another model is the so called "boosted Gaussian" wave function, for which

$$\phi_{T,L}(r,z) = \mathcal{N}_{T,L}z(1-z)\exp\left(-\frac{m_f^2\mathcal{R}^2}{8z(1-z)}-\frac{2z(1-z)r^2}{\mathcal{R}^2}+\frac{m_f^2\mathcal{R}^2}{2}\right). \quad (2.21)$$

In this case, for the J/Ψ meson, the parameters read [5] $M_V = 3.097$ GeV, $m_f = 1.4$GeV, $\mathcal{N}_T = 0.578$, $\mathcal{N}_L = 0.575$, $\mathcal{R}^2 = 2.3$ GeV^{-2} and $\delta = 1$.

Our numerical calculations showed that there is a difference of the order of 10% between the wave function models when calculating $\gamma^* p$ cross section. The difference is larger in the γ^*-nucleus cross section. However, the results obtained using both of these models are compatible within the experimental errors of the current HERA data shown in Fig. 8. We return to this topic later in Sec. 3.5. In the numerical calculations we used the "boosted Gaussian" parametrization.

From Eq. (2.7) we see that the $q\bar{q}p$ amplitude is multiplied by the factor $\frac{1}{2}r\int dz(\Psi^*\Psi)$. This quantity for the J/Ψ meson is plotted in Fig. 4, and as it can be seen, dipoles larger that $r \gtrsim 0.5$ fm are highly suppressed.

2.4 IPsat and IIM models

As it was discussed in Sec. 2.2, we need the dipole-proton cross section as a function of the impact parameter b_T. In this chapter we consider two popular models known as the IIM and IPsat models.

The IPsat model is obtained as follows [6]: from the lowest order pQCD calculations one can derive the cross section

$$\frac{\mathrm{d}\sigma_{q\bar{q}}}{\mathrm{d}^2 b_T} = \frac{\pi^2}{N_\mathrm{c}} r_T^2 \alpha_s(\mu^2) x_\mathbb{P} g(x_\mathbb{P}, \mu^2) \frac{T_p(b_T)}{2\pi B_p}, \tag{2.22}$$

where r_T is the transverse size of the dipole, $T_p(b_T)/(2\pi B_p)$ is the transverse profile of the gluon density of the proton normalized to unity and $x_\mathbb{P} g(x_\mathbb{P}, \mu^2)$ is the gluon density which evolves according to the DGLAP equation. The kinematical variable $x_\mathbb{P}$ is defined in Sec. 1.4.

From now on we assume that the proton shape is Gaussian, e.g. $T_p(b_T) = \exp(-b_T^2/(2B_p))$, and the evolution scale is taken to be $\mu^2 = C/r_T^2 + \mu_0^2$. In this work the parameters are taken to be $C = 4$ and $\mu_0^2 = 1.167$ GeV^2 following Ref. [5]. According to experimental results B_p is approximately constant in $\gamma^* p \to J/\Psi p$ scattering process and the value $B_p = 4.0$ GeV^{-2} is used as in Ref. [5].

Equation (2.22) is known as the IPnonsat model as it does not saturate at large dipole sizes but grows like r_T^2. This violates the the unitarity requirement of the scattering matrix introduced in Sec. 1.5. We will discuss this requirement in more detail in Sec. 2.5.

A straightforward way to generalize this result to take into account the required saturation at large dipoles is to exponentiate Eq. (2.22) to get

$$\frac{\mathrm{d}\sigma_{q\bar{q}}}{\mathrm{d}^2 b_T} = 2\left[1 - \exp\left(-r_T^2 F(x_\mathbb{P}, r_T) T_p(b_T)\right)\right], \tag{2.23}$$

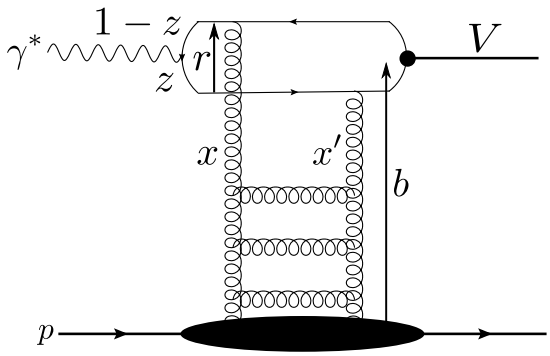

Figure 5. Dipole-proton scattering within the IPsat model with one gluon ladder.

with

$$F(x, r_T) = \frac{1}{2\pi B_p} \frac{\pi^2}{2N_c} \alpha_s(\mu^2) x_{\mathbb{P}} g(x_{\mathbb{P}}, \mu^2). \tag{2.24}$$

This result is known as the IPsat model. The interpretation of Eq. (2.23) is that the dipole interacts with the proton via two-gluon exchange (notice that we need at least two gluons as we are not allowed to exchange color charge with the proton). The quantum fluctuations inside the proton, described by the DGLAP evolution equation, generate a gluon cascade, and the exchanged gluons from the dipole couple with the produced gluon ladders. Exponentiation done in Eq. (2.23) sums over different number of gluon ladders $(1, 2, \dots)$. The situation with one ladder is shown in Fig. 5 [7].

Notice that the scattering amplitude saturates to 2 at large $|r_T|$ and it behaves like r_T^2 at small $|r_T|$. The contribution of large dipoles to the scattering amplitude is suppressed as the wave function overlap $\Psi_V^* \Psi$ decays exponentially at large $|r_T|$ as discussed in Sec. 2.3.

From Fig. 4 one can see that in a J/Ψ production we have to consider dipoles of the order of 1 GeV^{-1}, and with such a large dipoles the difference between the IPnonsat and the IPsat models is actually significant as it can be seen from Fig. 7. Thus one can expect to get too large cross sections when the IPnonsat model is used.

The second commonly used model is the so called IIM (Iancu, Itakura and Munier) model which is parametrized in such a way that it follows the energy dependence derived from perturbative QCD, namely the so called BK (Balitsky–Kovchegov) [8, 9] equation. The impact parameter dependence, however, is not derived from the BK equation, and in the IIM model it is

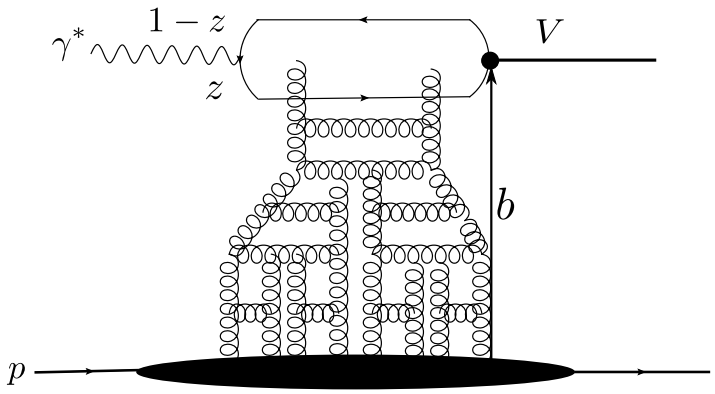

Figure 6. Dipole-proton scattering within the IIM model.

assumed to be factorized [10]:

$$\frac{\mathrm{d}\sigma_{q\bar{q}}}{\mathrm{d}^2 b_T} = 2T_p(b_T)\mathcal{N}(r_T, x_{\mathbb{P}}). \tag{2.25}$$

Here we have defined the saturation scale as

$$Q_s(x_{\mathbb{P}}) = \left(\frac{\mathrm{x}_0}{\mathrm{x}_{\mathbb{P}}}\right)^{\frac{\lambda}{2}} \text{ GeV} \tag{2.26}$$

and have written the amplitude $\mathcal{N}$ as

$$\mathcal{N}(rQ_s, x_{\mathbb{P}}) = \begin{cases} \left(\frac{rQ_s}{2}\right)^{2\gamma_c} \exp\left[-\frac{2\ln^2(rQ_s/2)}{\kappa\lambda\ln(1/x)}\right] & \text{for } rQ_s \leq 2 \\ 1 - e^{-4\alpha\ln^2(\beta rQ_s)} & \text{for } rQ_s > 2 \end{cases}. \tag{2.27}$$

The constants α and β are determined from the requirement that $\mathcal{N}$ and its derivative are continuous at $rQ_s = 2$, and for the rest of the constants we use the values given in Ref. [10]: $N_0 = 0.7$, $\kappa = 9.9$, $\gamma_c = 0.7376$, $\lambda = 0.2197$ and $x_0 = 1.632 \cdot 10^{-5}$. For the proton shape we use the result $B_p = 5.59$ GeV^{-2}.

The interpretation of the IIM model is shown in Fig. 6. In this case we look at the situation in target rest frame (TRF) in which the quantum fluctuations take place in the virtual photon wave function. In the TRF exchanged gluons emit more virtual gluons which interact with the proton. In the large N_c (number of colors) limit a radiated gluon is effectively replaced by an another $q\bar{q}$ dipole. The evolution then looks like that the original dipole splits into two new dipoles, which then split into more dipoles and so on. This evolution is described by the BK equation.

The parameter B_p describes the proton size. It is correlated with the other parameters in the IIM and IPsat models, so we do not alter the

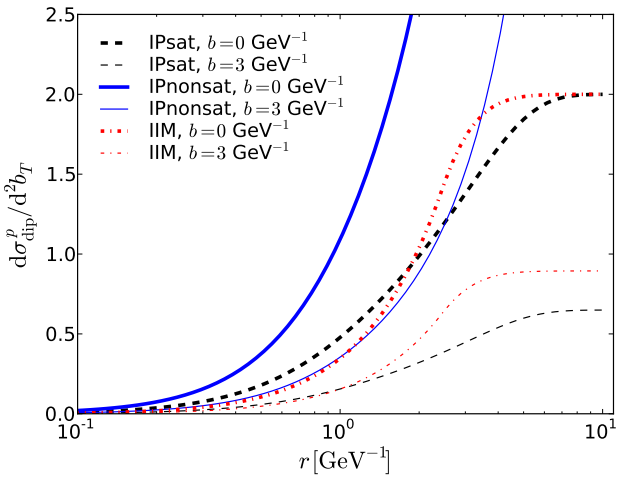

Figure 7. Impact-parameter dependent cross section for dipole-proton scattering in different models.

experimentally determined values and thus end up with using different proton shape in different models. However, as one can see in Fig. 8, both IIM and IPsat models describe the HERA data well.

There are also other ways to add the impact parameter dependence to the model obtained from the BK equation. One of these is the so called b-CGC model in which the b_T dependence is included in the saturation scale Q_s as [11]

$$Q_s(x) = \left(\frac{x_0}{x_{\mathbb{P}}}\right)^{\frac{\lambda}{2}} T_p(b_T)^{\frac{1}{2\gamma_s}}. \tag{2.28}$$

In our work we didn't study this model in detail.

For computational simplicity we approximated that we can also factorize the impact parameter dependence of the IPsat model and write Eq. (2.23) as

$$\frac{\mathrm{d}\sigma_{q\bar{q}}}{\mathrm{d}^2b_T} = 2T_p(b_T)\left[1 - \exp\left(-r_T^2 F(x_{\mathbb{P}}, r)\right)\right]. \tag{2.29}$$

This approximation brings the IPsat parametrization to the same form as the IIM parametrization, Eq. (2.25), with $\mathcal{N}(r_T, x) = 1 - \exp(-r^2F(x, r_T))$. In this approximation one can calculate the scattering amplitude from Eq. (2.12) to be

$$-i\mathcal{A}_{q\bar{q}}(x_{\mathbb{P}}, r_T, \Delta_T) = 4\pi B_p \mathcal{N}(r_T, x_{\mathbb{P}}) e^{-B_p\Delta_T^2/2}. \tag{2.30}$$

Even though the unfactorized IPsat dipole cross section (2.23) gives the correct unitarity limit at all impact parameters and the factorized one doesn't,

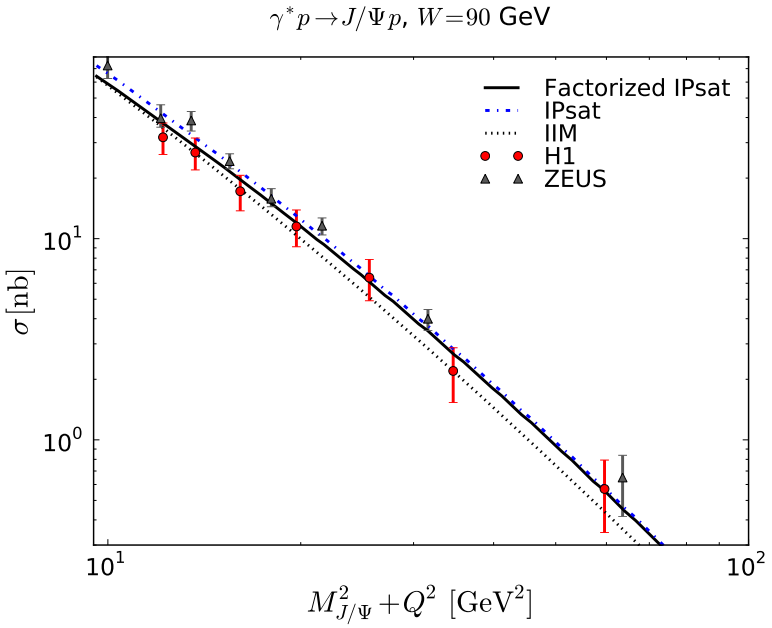

Figure 8. Comparison of the used dipole cross sections to HERA data [12, 13] on diffractive J/Ψ production.

there seems to be little difference between these models when describing the HERA data as can be seen from Fig. 8. Thus from now on we limit our study to the factorized version of the IPsat model.

2.5 Saturation and unitarity requirement

Conservation of probability, or the unitarity of the S matrix, requires that there is an upper bound for the elements of the S matrix as discussed in Sec. 1.5: $S \leq 1$. Comparing this and Eq. (2.11) one can see that the maximum value of $\mathrm{d}\sigma_{q\bar{q}}/\mathrm{d}^2 b_T$ is 2. This is the unitarity limit of the scattering amplitude which leads to the saturation: at large dipoles the cross section must saturate to 2. The IPnonsat model, Eq. (2.22), violates this requirement as the cross section always grows like r_T^2.

We can understand the physical phenomenon behind this mathematical treatment by considering the number and size of the gluons inside the proton. Working still in the target rest frame in which the dipole model was derived, it is intuitively clear (and it can also be seen from the scattering amplitude of the IPsat model, Eq. (2.23)) that the cross section grows when the number of gluons seen inside the proton grows.

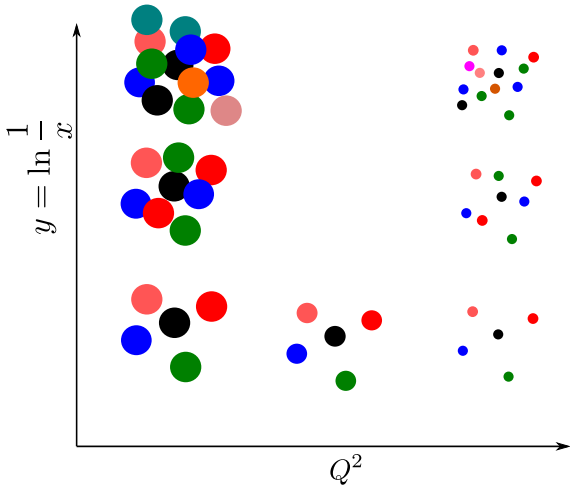

Figure 9. Gluons in y, Q^2 plane. As rapidity y increases, the number of gluons with apparent size $1/Q^2$ increases.

As the dipole size is approximately $1/Q$, the area of a single gluon seen by the dipole is of the order of $1/Q^2$, and the number of these gluons is $xg(x, \mu^2)$. The gluons do not overlap when the dipole size $(1/Q)$ is small and there are only a few gluons, meaning that x is large. In this limit the cross section grows linearly as a function of xg. This is exactly what we get by expanding IPsat model, Eq. (2.23), to lowest order in xg (IPnonsat model). The situation is shown schematically in Fig. 9.

The nonlinear effects in Eq. (2.23) become important when $r_T^2 F(x_{\mathbb{P}}, r_T)$ is of the order of 1. This corresponds the case in which

$$1 \sim \frac{r_T^2 \alpha_s xg}{B_p} \approx \frac{\alpha_s xg}{Q^2 R_p^2}. \tag{2.31}$$

Here R_p is the proton radius. The interpretation of this result is clear: $1/Q^2$ is the area of the gluon, so the nonlinear effects become important when the total area of the gluons seen by the dipole is of the order of the proton area. An extra factor α_s follows from the fact that actually the nonlinearities follow from the gluon recombination whose rate is set by the strong coupling constant.

2.6 Corrections due to the real part of the scattering amplitude and the skewedness effect

When deriving Eq. (2.11) we assumed that the S matrix is completely real, which means that the scattering amplitude is purely imaginary. To get more accurate results we can also take into account the real part of the amplitude by computing the ratio between the real and the imaginary part of the scattering amplitude denoted by β. The result is [11]

$$\beta = \tan\left(\frac{\pi\lambda}{2}\right), \text{ with} \quad \lambda = \frac{\partial \ln \mathcal{A}_{T,L}^{\gamma^* p \to Vp}(x, Q^2, \Delta_T)}{\partial \ln(1/x)}. \tag{2.32}$$

In addition we also have to take into account that the gluons emitted from the quark and the antiquark carry different momentum fractions x. This is known as the skewedness effect, and it can be taken into account by computing the correction factor R_g, which is [14]

$$R_g(\lambda) = \frac{2^{2\lambda+3}}{\sqrt{\pi}} \frac{\Gamma(\lambda + 5/2)}{\Gamma(\lambda + 4)}. \tag{2.33}$$

Taking into account both correction factors the cross section for $\gamma^* p \to Vp$ scattering, Eq. (2.8), becomes

$$\frac{\mathrm{d}\sigma_{\gamma^* p}}{\mathrm{d}t} = \frac{R_g^2(1+\beta^2)}{16\pi} |\mathcal{A}_{\gamma^* p}(x, r, \Delta_T)|^2. \tag{2.34}$$

Numerical calculations show that the real part correction increases the cross section 5–10% and the skewedness effect about 30%. Thus these corrections must be taken into account when comparing the results with the measured absolute cross section. These corrections are included in Fig. 8 where the numerical results are compared with the measurements.

It is not completely clear how these factors should be generalized in dipole-nucleus scattering. As a first order approximation we computed the corrections from the dipole-proton cross section.

2.7 ϕ and ρ meson production

The impact parameter b_T is assumed to be the Fourier conjugate of the momentum transfer Δ_T in Eq. (2.12). It has been argued that according to the explicit QCD calculations the momentum transfer Δ_T should conjugate with $b_T + (1-z)r_T$ [5]. Geometrically $b_T + (1-z)r_T$ is the distance from the

center of mass of the proton to one of the two quarks, see Fig. 5. In this case the dipole amplitude, Eq. (2.12), becomes

$$\mathcal{A}_{q\bar{q}}(x, r_T, \Delta_T) = i \int \mathrm{d}^2 b_T e^{-i[b_T + (1-z) r_T] \cdot \Delta_T} \frac{\mathrm{d}\sigma_{q\bar{q}}}{\mathrm{d}^2 b_T}. \tag{2.35}$$

All measured diffractive vector meson production cross sections are well described by the exponential dependence $d\sigma/dt \sim \exp(-B_D|t|)$ [5]. Now if Eq. (2.35) is used when the $\gamma^* p$ cross section is calculated, the slope B_D is no longer the same as the proton slope parameter B_p even if the factorized amplitude, Eq. (2.25), is used. Instead the slope also depends on r_T, and thus on $Q^2 \sim 1/r_T^2$.

The slope B_D can be interpreted as a measure of the size of the interaction area [5]. As we are interested in J/Ψ production where the average dipole size is much smaller than the proton radius (see Fig. 4), the correction included in Eq. (2.35) can be neglected. Thus we compute the dipole-proton amplitude by using Eq. (2.12), and the slope $B_D = B_p$ and it does not depend on Q^2.

For larger mesons, such as ϕ and ρ, the experimentally measured B_D is significantly larger than the fitted value of B_p and depends on Q^2. In these cases one can still use fixed B_p together with Eq. (2.35) to obtain a good description of the experimental data [5].

2.8 From $\gamma^* p$ scattering to ep scattering

So far we have considered only $\gamma^* p$ scattering, but this is not what we see in experiments. Actually one could argue that the $\gamma^* p$ cross section is not even a well-defined concept as the virtual photon flux is arbitrary. However the role of the electron beam in the scattering process is just to act as a source of (virtual) photons, so it can be replaced by an equivalent virtual photon flux.

The idea is to calculate the cross section for $ep \to X$ and $\gamma p \to X$ processes in terms of the components of the hadronic tensor $W^{\mu\nu}$. Combining these two expressions one notices that the flux factor in γp scattering is proportional to the photon energy $K = \nu$ in the target rest frame. On the other hand the invariant mass squared of the final state is $W^2 = (p+q)^2 = M^2 + 2MK$, where M is the proton mass, p is the proton momentum and q is the photon momentum. This result is generalized to cover also virtual photons by requiring that K always satisfies this equation, leading to the requirement [15]

$$K = \frac{W^2 - M^2}{2M} = \nu + \frac{q^2}{2M}. \tag{2.36}$$

As a result one finds that the ep cross section can be expressed in terms

of longitudinal (L) and transverse (T) $\gamma^* p$ cross sections as [16]

$$\frac{\mathrm{d}\sigma^{ep\to eJ/\Psi p}}{\mathrm{d}y\mathrm{d}Q^2} = \Gamma(\sigma_T^{\gamma^* p\to J/\Psi p} + \epsilon\sigma_L^{\gamma^* p\to J/\Psi p}). \tag{2.37}$$

The virtual photon flux factor Γ is

$$\Gamma = \frac{\alpha_{\mathrm{em}}(1-y+y^2/2)}{\pi y Q^2}, \tag{2.38}$$

and

$$\epsilon = \frac{2(1-y)}{1+(1-y)^2}. \tag{2.39}$$

Kinematical variable y is defined as

$$y = \frac{p\cdot q}{p\cdot k}, \tag{2.40}$$

and its interpretation is that it gives the fraction of the electron energy carried by the exchanged photon in the proton rest frame. The average value of ϵ in the kinematical region studied in HERA is approximately 0.99 [12].

We can conclude that it is quite easy to compute ep cross section from the $\gamma^* p$ cross section: we only have to multiply it by a flux factor Γ which depends on the kinematics. This allows us to study the $\gamma^* p$ and $\gamma^* A$ scatterings which contain all the interesting physics related to the scattering processes.

3 Nuclear suppression

Dipole-nucleus scattering is interesting because nucleons inside the nucleus are not independent. So we expect to see some contribution from the nuclear structure in the cross section. These nuclear effects can be used to study, for example, the properties of the nucleus.

3.1 Dipole-nucleus scattering

In case of dipole-nucleus scattering one can find two different types of events. In coherent scattering the nucleus stays intact meaning that it remains in its ground state. On the other hand in incoherent scattering nucleus is allowed move to an excited state or to break up into smaller color-free nuclei. We define quasi-elastic process so that both coherent and incoherent scattering events are allowed.

We generalize our results from dipole-proton scattering by writing the S matrix for dipole-nucleus scattering as

$$S_A(r_T, b_T, x) = \prod_{i=1}^{A} S_p(r_T, b_T - b_{T_i}, x). \tag{3.1}$$

A justification for this is that the matrix element S_p gives the probability that the dipole does not scatter off the proton and we have assumed that the scattering events are independent. Here b_{T_i} are the nucleon transverse coordinates, b_T is the impact parameter and S_p is the scattering matrix for the dipole-proton scattering. This makes it possible to get the scattering amplitude for dipole-nucleus scattering, as the S matrix is related to scattering amplitude via the T matrix defined as $S = 1 + iT$, and $\mathcal{A}(i \to j) = T_{ij}$. Thus $-i\mathcal{A} = 1 - S$.

When considering dipole-nucleus scattering the amplitude must be averaged over all possible nucleon configurations. For this purpose we define nucleon wave function ψ such that $[\psi^*\psi](r_1, \ldots, r_A)$ is the probability to find nucleons at positions $r_1, \ldots, r_A$. Here A is the number of nucleons in the nucleus. We neglect the nucleon-nucleon correlations and assume that the positions of the nucleons are independent, meaning that we can write

$$[\psi^*\psi](r_1, \ldots, r_A) = \prod_{i=1}^{A} \rho(r_i). \tag{3.2}$$

Here ρ is the density of nucleons inside the nucleus which is usually assumed

to follow the Woods-Saxon distribution [17]:

$$\rho_{WS}(r) = \frac{N}{\exp\left(\frac{r-R_A}{\delta}\right)+1}, \tag{3.3}$$

where constants $R_A = 1.12\ \text{fm}A^{1/3} - 0.86\ \text{fm}A^{-1/3}$ and $\delta = 0.54$ fm are taken to be same as in Ref. [18] and N normalizes the number of nucleons to unity: $\int \mathrm{d}^3 r \rho_{WS}(r) = 1$.

The effect of two-body correlations is not something we can simply argue to be small, and on the other hand diffractive scattering processes might give us a good way to study these correlations as suggested by Caldwell and Kowalski [18]. However the result of Ref. [18] is derived using the IPnonsat model and then linearizing the $\gamma^* A$ amplitude as we shall discuss in more detail later in this chapter when we derive Eq. (3.20). As it was shown in Sec. 2.4, IPnonsat model gives a too large cross section and thus the result of Ref. [18] for the two-body correlations is not realistic. The effect of nucleon correlations in IPsat or IIM model was out of the scope of this research and is left for future work.

Due to the strong Lorentz contraction we can integrate out the longitudinal dimension and define the transverse density of the nucleus as

$$T_A(b_T) = T_{WS}(b_T) = \int_{-\infty}^{\infty} \mathrm{d}z \rho_{WS}\left(\sqrt{z^2 + b_T^2}\right). \tag{3.4}$$

The function T_{WS} for a few different nuclei is shown in Fig. 10.

Let us then derive the scattering amplitude for dipole-nucleus scattering. In this case we must average over the nucleon configurations and, in case of incoherent scattering, sum over possible final states. The average over nucleon positions is denoted here by

$$\langle \mathcal{O}(\{b_{T_i}\})\rangle_N = \int \prod_{i=1}^{A} \left[\mathrm{d}^2 b_{T_i} T_A(b_{T_i})\right] \mathcal{O}(\{b_{T_i}\}). \tag{3.5}$$

Let us first consider coherent scattering where the final state is the same as the initial state. This allows us to directly write the scattering amplitude according to Eqs. (2.8) and (2.7):

$$\begin{aligned}\frac{\mathrm{d}\sigma^{\gamma^* A\to J/\Psi A}}{\mathrm{d}t} = \frac{1}{16\pi}\left|\langle \mathcal{A}^A(x,Q^2,\Delta_T)\rangle_N\right|^2 = \frac{1}{16\pi}\Bigg| \int \mathrm{d}^2 r_T \frac{\mathrm{d}z}{4\pi} [\Psi_V^* \Psi]_{T,L}(r_T, z, Q) \\ \times \int \prod_{i=1}^{A} \left[\mathrm{d}^2 b_{T_i} T_A(b_{T_i})\right] \int \mathrm{d}^2 b_T e^{-i b_T \cdot \Delta_T} \frac{\mathrm{d}\sigma_{q\bar{q}}^A}{\mathrm{d}^2 b_T}(\{b_{T_i}\})\Bigg|^2 .\end{aligned} \tag{3.6}$$

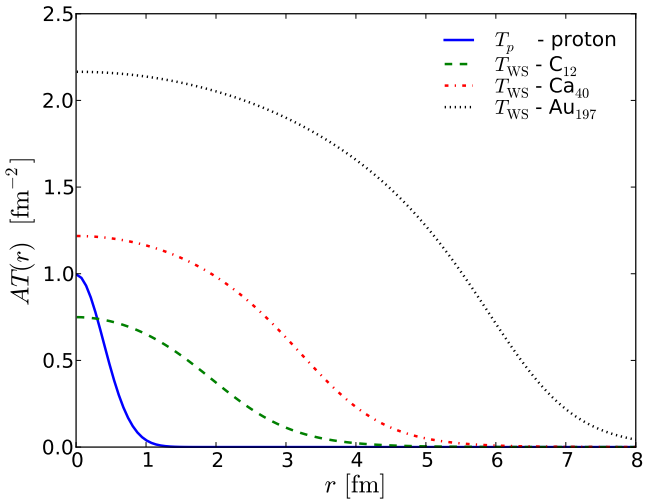

Figure 10. Transverse nuclear density for a few different nuclei using the Woods-Saxon distribution.

This expression turns out to be simple enough to calculate also in the non-factorized IPsat model as the average is calculated at the level of the scattering amplitude [6]. In the limit of a large and smooth nucleus the result is

$$\begin{aligned}\langle \mathcal{A}^A(x,Q^2,\Delta_T)\rangle_N = i\int \frac{\mathrm{d}z}{4\pi}\mathrm{d}^2r_T\mathrm{d}^2b_T e^{-ib_T\cdot\Delta_T}[\Psi_V^*\Psi](r_T,Q^2) \\ \times 2\left[1-\exp\left\{-\frac{1}{2}\sigma^p_{q\bar{q}}AT_A(b)\right\}\right].\end{aligned} \tag{3.7}$$

If the impact parameter dependence is factorized, $\sigma^p_{q\bar{q}}$ can be evaluated to be

$$\sigma^p_{q\bar{q}} = \int \mathrm{d}^2b_T 2T_p(b_T)\mathcal{N} = 4\pi B_p\mathcal{N}. \tag{3.8}$$

We discuss the smooth nucleus approximation in more detail later in this chapter.

However when we consider the incoherent scattering it turns out that the situation is more difficult. This is due to the fact that now we must calculate the average at the level of the cross section. We see this by denoting the initial state by A_0, the final state by A_f (now $f \neq 0$) and the T-matrix by T

and using the completeness relation:

$$\begin{aligned}\sum_{f\neq 0}|\langle A_0|T|A_f\rangle|^2 &= \sum_f |\langle A_0|T|A_f\rangle|^2 - |\langle A_0|T|A_0\rangle|^2 \\ &= \langle A_0|T|\sum_f A_f\rangle\langle A_f|T^\dagger|A_0\rangle - |\langle A_0|T|A_0\rangle|^2 \\ &= \langle A_0|\,|T|^2\,|A_0\rangle - |\langle A_0|T|A_0\rangle|^2.\end{aligned} \tag{3.9}$$

Thus in terms of dipole-nucleus scattering amplitude $\mathcal{A}^A_{q\bar{q}}$ we can write the amplitude squared for the incoherent scattering as a variance $\langle|\mathcal{A}^A_{q\bar{q}}|^2\rangle_N - |\langle\mathcal{A}^A_{q\bar{q}}\rangle_N|^2$. Moreover we notice that $|\langle\mathcal{A}^A_{q\bar{q}}\rangle_N|^2$ is the scattering amplitude for coherent dipole-nucleus scattering, see Eq. (3.6).

As the coherent scattering amplitude, Eq. (3.7), is proportional to the Fourier transform of a smooth function, its contribution to the quasielastic scattering amplitude vanishes when $\Delta \gtrsim 1/R_A$. Therefore at large Δ the quasielastic cross section is almost purely incoherent.

To get the quasielastic scattering amplitude we must average the squared amplitude over different nucleon configurations. The calculation is quite straightforward but also a bit laborious. We begin this by writing

$$\begin{aligned}\langle|\mathcal{A}^A_{q\bar{q}}|^2\rangle_N = 4\int\prod_{i=1}^{A}\left[\mathrm{d}^2b_{T_i}T_A(b_{T_i})\right]\mathrm{d}^2b_T\mathrm{d}^2b'_T e^{-i(b_T-b'_T)\cdot\Delta_T} \\ \times\left[1-\prod_{j=1}^{A}(1-\mathcal{N}(r_T)T_p(b_T-b_{T_j}))\right]\left[1-\prod_{k=1}^{A}(1-\mathcal{N}(r'_T)T_p(b'_T-b_{T_k}))\right]\end{aligned} \tag{3.10}$$

One can then proceed by expanding the product and calculating the Gaussian integrals. The term containing $T_p(b_T-b_{T_l})T_p(b_T-b_{T_l})$ can be integrated by noticing that

$$T_p(b_T-b_{T_l})T_p(b'_T-b_{T_l}) = \exp\left(-\frac{2(b_{T_l}-\frac{1}{2}(b_T+b'_T))^2+\frac{1}{2}(b_T-b'_T)^2}{2B_p}\right), \tag{3.11}$$

and making the change of variable to $b'_{T_l} = b_{T_l} - \frac{1}{2}(b_T+b'_T)$. Integrals can be calculated analytically when one also takes into account the smooth nucleus approximation. This follows from the fact that $T_p(b_{T_i}) \approx 0$ when $b_{T_i} \gtrsim 1$ fm, and $T_A(b_T)$ changes slowly within a lengths comparable to the proton size, and thus

$$\int \mathrm{d}^2b_{T_i}T_A(b_{T_i})T_p(b_T-b_{T_i}) \approx T_A(b_T)\int\mathrm{d}^2b'_{T_i}T_p(b'_{T_i}) = 2\pi B_pT_A(b_T). \tag{3.12}$$

This approximation was also used when the coherent scattering amplitude, Eq. (3.7), was derived. These calculations lead to the expression

$$\begin{aligned}\langle|\mathcal{A}^A_{q\bar{q}}|^2\rangle_N = 4\int \mathrm{d}^2b_T\mathrm{d}^2b'_T e^{-i(b_T-b'_T)\cdot\Delta}\Bigg[1-(1-2\pi B_p\mathcal{N}(r_T)T_A(b_T))^A \\ -(1-2\pi B_p\mathcal{N}(r'_T)T_A(b'_T))^A+\Bigg(1-2\pi B_p(\mathcal{N}(r_T)T_A(b_T)+\mathcal{N}(r'_T)T_A(b'_T)) \\ +\pi B_p\mathcal{N}(r_T)\mathcal{N}(r'_T)e^{-(b_T-b'_T)^2/(4B_p)}T_A\left(\frac{1}{2}(b_T+b'_T)\right)\Bigg)^A\Bigg].\end{aligned} \tag{3.13}$$

We can then continue by making the change of variables to $b_1 = b_T - b'_T$ and $b_2 = \frac{1}{2}(b_T + b'_T)$. As we have a highly oscillatory prefactor $e^{-ib_1\cdot\Delta}$ and we are mainly interested in the high Δ region, we can neglect the terms not containing $e^{-b_1^2}$ due to the strong suppression. So we can neglect everything but the last $(\dots)^A$ term which we write using the binomial factor. We then get the result by using again the smoothness of the T_A, namely $T_A(\frac{1}{2}(b_1+2b_2)) \approx T_A(b_2)$ as we can assume b_1 to be small compared to the b_2 due to the strong suppression at large b_1. Putting all these together gives

$$\begin{aligned}\langle|\mathcal{A}^A_{q\bar{q}}|^2\rangle_N = 4\int \mathrm{d}^2b_1\mathrm{d}^2b_2 e^{-ib_1\cdot\Delta_T}\sum_{n=1}^{A}\binom{A}{n}e^{-nb_1^2/(4B_p)} \\ \times\left(1-2\pi B_pT_A(b_2)[\mathcal{N}(r_T)+\mathcal{N}(r'_T)]\right)^{A-n}\left(T_A(b_2)\pi B_p\mathcal{N}(r_T)\mathcal{N}(r'_T)\right)^n.\end{aligned} \tag{3.14}$$

By calculating the b_1 integral, writing $()^{A-n} = ()^A()^{-n}$ and taking the limit of large A we can then write

$$\begin{aligned}\langle|\mathcal{A}^A_{q\bar{q}}|^2\rangle_N = 16\pi B_p\int \mathrm{d}^2b_2\sum_{n=1}^{A}\binom{A}{n}\frac{1}{n}e^{-B_p\Delta^2/n} \\ \times e^{-A2\pi B_pT_A(b_2)[\mathcal{N}(r_T)+\mathcal{N}(r'_T)]}\left(\frac{\pi B_p\mathcal{N}(r_T)\mathcal{N}(r'_T)T_A(b_2)}{1-2\pi B_pT_A(b_2)[\mathcal{N}(r_T)+\mathcal{N}(r'_T)]}\right)^n.\end{aligned} \tag{3.15}$$

We have verified numerically that terms with $n \geq 2$ do not contribute much at the values of t we are interested in (the $n = 2$ contribution is typically $\lesssim 2\%$ reaching 5% at $|t| \gtrsim 0.5$ GeV^2) so we can take into account only the

case with $n = 1$. Thus the final result is (writing $b_T = b_2$)

$$\langle |\mathcal{A}^A_{q\bar{q}}|^2 \rangle_N = 16\pi B_p A \int \mathrm{d}^2 b_T e^{-B_p \Delta_T^2} \times e^{-A 2\pi B_p T_A(b_T)[\mathcal{N}(r_T)+\mathcal{N}(r'_T)]} \left(\frac{\pi B_p \mathcal{N}(r_T)\mathcal{N}(r'_T) T_A(b_T)}{1 - 2\pi B_p T_A(b_T)[\mathcal{N}(r_T) + \mathcal{N}(r'_T)]} \right)^n . \tag{3.16}$$

A similar expression is also derived in Ref. [19].

Notice that in this case we have to calculate the product of the amplitude (2.7) and its complex conjugate in order to get the total cross section, so we have to integrate over r_T and r'_T. The differential cross section for $\gamma^* A \to J/\Psi A$ scattering at large Δ_T is then

$$\frac{\mathrm{d}\sigma^{\gamma^* A \to J/\Psi A}}{\mathrm{d}t} = \frac{1}{16\pi} \int \frac{\mathrm{d}z}{4\pi} \frac{\mathrm{d}z'}{4\pi} \mathrm{d}^2 r_T \, \mathrm{d}^2 r'_T [\Psi^*_V \Psi](r_T, z, Q)[\Psi^*_V \Psi](r'_T, z', Q) \times \left\langle |\mathcal{A}^A_{q\bar{q}}|^2 (x, r_T, r'_T, \Delta_T) \right\rangle_N \tag{3.17}$$

We return to the interpretation of this result in Sec. 3.5.

For comparison we shall also consider the dipole-nucleus scattering using the IPnonsat model (Eq. (2.22)) for dipole-proton scattering. We also expand the product of S matrices, Eq. (3.1), to the lowest order in the scattering amplitude as it is done e.g. in Ref. [18]. This approximation means that we ignore multiple scattering events and leads to the result

$$\frac{\mathrm{d}\sigma^A_{q\bar{q}}}{\mathrm{d}^2 b_T}(\{b_{T_i}\}) = \mathcal{N}_{\mathrm{nonsat}}(r_T) \sum_i T_p(b_T - b_{T_i}), \tag{3.18}$$

with

$$\mathcal{N}_{\mathrm{nonsat}}(r_T) = \frac{\pi^2}{2N_\mathrm{c}} \frac{1}{2\pi B_p} r_T^2 \alpha_s(\mu^2) x_{\mathbb{P}} g(x_{\mathbb{P}}, \mu^2). \tag{3.19}$$

Notice that this approximation is much worse than what was done with the IPsat and IIM models before. Now we just assume that the dipole scatters only off one nucleon, so we can just sum these amplitudes. Our approach with IPsat and IIM models was more realistic, as we calculated product of the S matrix element which still allows the dipole to scatter off multiple nucleons (notice that S matrix essentially tells us the probability to not to scatter).

In the IPnonsat model the nice result is that the incoherent dipole-nucleus cross section turns out to be exactly A times that of the proton at large t.

This can be seen from the quasi-elastic scattering amplitude

$$\langle|\mathcal{A}^A_{q\bar{q}}|^2\rangle_N = \mathcal{N}^2_{\text{nonsat}}(r_T)e^{-B_p\Delta^2}\left[A + A(A-1)\left|\int \mathrm{d}^2b_T e^{-ib_T\cdot\Delta_T}T_A(b_T)\right|^2\right], \tag{3.20}$$

where the Fourier transformation is small at large Δ_T. Moreover, the squared amplitude for the coherent scattering turns out to be

$$|\langle\mathcal{A}^A_{q\bar{q}}\rangle_N|^2 = A^2\mathcal{N}^2_{\text{nonsat}}(r_T)e^{-B_p\Delta^2}\left|\int \mathrm{d}^2b_T e^{-ib_T\cdot\Delta_T}T_A(b_T)\right|^2. \tag{3.21}$$

The cross section for incoherent scattering can then be derived by subtracting Eq. (3.21) from Eq. (3.20). Notice that the coherent cross section at $t = 0$ is exactly A times the the incoherent one extrapolated to $t = 0$. Numerical results for the cross section using different models are plotted in Fig. 11 and discussed in more detail in Secs. 3.3 and 3.5.

3.2 Numerical computations

In order to study the nuclear suppression in more detail we calculated numerically the differential cross sections for both γ^*-proton and γ^*-nucleus scattering processes. In these calculations the approximation that we can write the IPsat model in factorized form, Eq. (2.29), is crucial. In case of incoherent scattering this approximation allowed us to calculate the Fourier transformation analytically, and at the end there is only one integral in the squared dipole-nucleus scattering amplitude which must be computed numerically. In non-factorized case we would have to compute the Fourier transform numerically with different nucleon configurations which would be much more demanding.

Numerical results are calculated by using a software written as a part of this research training. The software is written in C++ and uses GSL (GNU Scientific Library) for numerical calculations. IPsat model requires the gluon distribution of the proton, namely function $xg(x, \mu^2)$. This is obtained from Ref. [5]. The code uses tabulated values for function $\alpha_s xg(x, \mu^2)$, and interpolates that function between the data points linearly as a function of x and using the interpolation routines of the GSL as a function of the dipole size. The code is released as a free software and can be downloaded from http://yousource.it.jyu.fi/diffractive-ea.

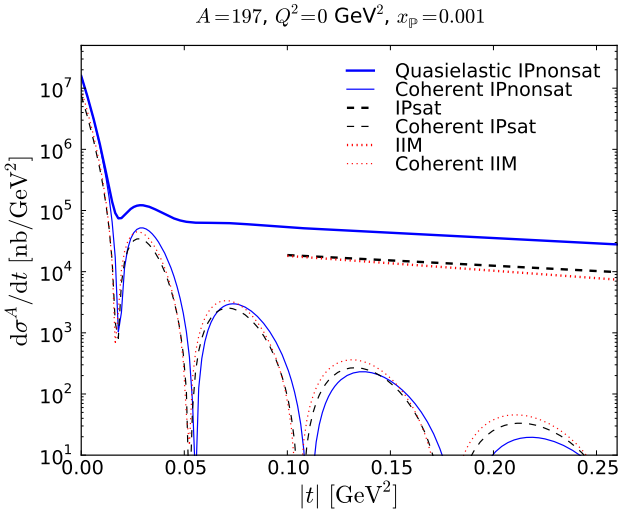

Figure 11. The quasielastic and coherent diffractive $\gamma^* A \to J/\Psi A$ cross sections in gold nuclei. Our approximation for the quasielastic cross section for the IPsat and IIM models, Eq. (3.22), is valid in large $|t|$ region.

3.3 Incoherent dipole-nucleus scattering

The main theoretical result of this work is Eq. (3.16),

$$\begin{aligned}\langle|\mathcal{A}^A_{q\bar{q}}|^2\rangle_N = 16\pi B_p A \int \mathrm{d}^2 b_T e^{-B_p\Delta_T^2} \pi B_p \mathcal{N}(r_T)\mathcal{N}(r'_T) T_A(b_T) \\ \times \frac{e^{-A2\pi B_p T_A(b_T)[\mathcal{N}(r_T)+\mathcal{N}(r'_T)]}}{1-2\pi B_p T_A(b_T)[\mathcal{N}(r_T)+\mathcal{N}(r'_T)]},\end{aligned} \tag{3.22}$$

which gives the differential cross section for $q\bar{q}A \to J/\Psi A$ scattering at large $|t|$. The differential cross sections computed from Eq. (3.22) (inelastic) and Eq. (3.6) (elastic) are shown in Fig. 11 in case of gold nucleus ($A = 197$). For comparison the results obtained from the IPnonsat model, namely from equations (3.20) for quasi-elastic scattering and (3.21) for coherent scattering, are also shown.

Comparing equation (3.22) with the result obtained for the dipole-proton scattering in section 2.4, Eq. (2.30), one can see that the squared amplitude in incoherent dipole-nucleus scattering is proportional to A times the squared amplitude for a dipole scattering off a proton, which corresponds to the dipole scattering independently off the nucleons in a nucleus. This is then multiplied

by a nuclear attenuation factor

$$\frac{e^{-2\pi B_p A T_A(b_T)[\mathcal{N}(r_T)\mathcal{N}(r'_T)]}}{1-2\pi B_p T_A(b_T)[\mathcal{N}(r_T)+\mathcal{N}(r'_T)]} \approx e^{-2\pi B_p T_A(b_T)(A-1)[\mathcal{N}(r_T)+\mathcal{N}(r'_T)]}. \quad (3.23)$$

The exponent in the suppression factor is proportional to $B_p\mathcal{N}(r_T)$ which gives the total (not elastic) dipole-proton cross section: $\sigma^p_{q\bar{q}}(r_T, x) = 4\pi B_p \mathcal{N}(r_T, x_{\mathbb{P}})$. Notice the difference when compared with the total elastic cross section which is $\pi B_p \mathcal{N}(r_T, x_{\mathbb{P}})^2$. The attenuation factor takes into account the fact that the dipole must not scatter inelastically off the other $A-1$ nucleons to keep the event diffractive, and it can be interpreted as the probability for a dipole, with a cross section which is the average of dipoles with sizes r_T and r'_T, to pass though the nucleus.

As one can clearly see from Fig. 11, the IPnonsat model significantly overestimates the cross section, as in that model the dipole-proton scattering amplitude does not saturate and, in addition, the nuclear suppression is not taken into account.

As it was discussed in Sec. 2.4, in IPnonsat model the coherent cross section at $t = 0$ is exactly A times the incoherent one extrapolated to $t = 0$. To see the effect of nuclear suppression we computed this factor also for IPsat and IIM models: in the IPsat model we got 270 (250) and in the IIM model 300 (270) at $Q^2 = 0$ ($Q^2 = 10$ GeV^2) with $A = 197$.

3.4 Cross section in the black disk and dilute limits

As we saw in the previous chapter, there is a nuclear suppression factor in the dipole-nucleus scattering amplitude, Eq. (3.23). The source of this factor can be understood by considering scattering off the nucleus in different limits.

Let us consider an elementary probe (virtual photon) scattering off the nucleus. In the dilute limit (where the virtuality Q^2 of the virtual photon is large) the wavelength of the probe in the transverse direction is so small that it sees all the nucleons inside the nucleus independently. Thus the cross section is proportional to the number of nucleons A.

However in the black disk limit, in which the probe always scatters off the nucleus, the situation is different. We saw in Sec. 3.1 that the scattering amplitude squared for the incoherent scattering is the variance of $\mathcal{A}$, $\langle|\mathcal{A}|^2\rangle - |\langle\mathcal{A}\rangle|^2$. When computing the total cross section, the impact parameter dependence must be integrated out, so

$$\sigma^{\text{incoh}}_{q\bar{q}} \sim \int \mathrm{d}^2 b_T \left(\langle|\mathcal{A}|^2\rangle - |\langle\mathcal{A}\rangle|^2\right). \quad (3.24)$$

As the probe always scatters, there are no fluctuations in $\mathcal{A}$ inside or outside the nucleus, so the variance of $\mathcal{A}$ must be zero in these regions. Thus the incoherent scattering can only happen on the surface (with thickness d) of the nucleus, and it behaves like

$$\sigma_{q\bar{q}}^{\text{incoh}} \sim 2\pi R_A d \sim A^{1/3}. \tag{3.25}$$

Notice that in the IPnonsat model we summed the amplitudes for the dipole to scatter off every single nucleon, which means that we worked in the dilute limit. As a result we derived the equations (3.20) and (3.21), from which one can clearly see that the incoherent cross section is exactly proportional to A. However when we derived the result for IPsat and IIM models we did not work in the dilute limit, and thus the strong suppression is expected. We would reach the dilute limit only at very large values of Q^2 which would correspond to small dipoles. We will discuss this limit more in Sec. 3.5.

3.5 Nuclear suppression as a function of $x_{\mathbb{P}}$, Q^2 and A

In order to see the effect of the nuclear suppression and its dependence on the kinematical variables we studied the ratio of the cross sections for the scattering off the gold nucleus compared with A times the cross section off the proton. More formally, we computed the ratio

$$\frac{\mathrm{d}\sigma^A/\mathrm{d}t}{A\mathrm{d}\sigma^p/\mathrm{d}t} \tag{3.26}$$

as a function of Q^2 and $x_{\mathbb{P}}$ for the incoherent $\gamma^* A \to J/\Psi A$ scattering. This quantity is sometimes called as the "nuclear transparency".

It is also more accurate to study the ratio of the cross sections than their absolute values, as the skewedness factor and the real part of the scattering amplitude affect on the absolute value, but in our approximation they cancel out when considering the ratio. As discussed in Sec. 2.6, it is not completely clear how these corrections should be computed for dipole-nucleus scattering, so it is good to be able to cancel out these somehow uncertain factors.

The nuclear suppression factor as a function of $M_{J/\Psi}^2 + Q^2$ is plotted in Fig. 12. The suppression is very large as expected, as the cross section behaves like $\sim A^{1/3}$ in the black disk limit. The suppression factor approaches unity at large values of Q^2 as the dipole size decreases, but the suppression is still quite significant at $Q^2 = 100$ GeV^2 which is the expected upper bound for Q^2 in a proposed eRHIC electron-ion collider at $x \lesssim 10^{-3}$ [2].

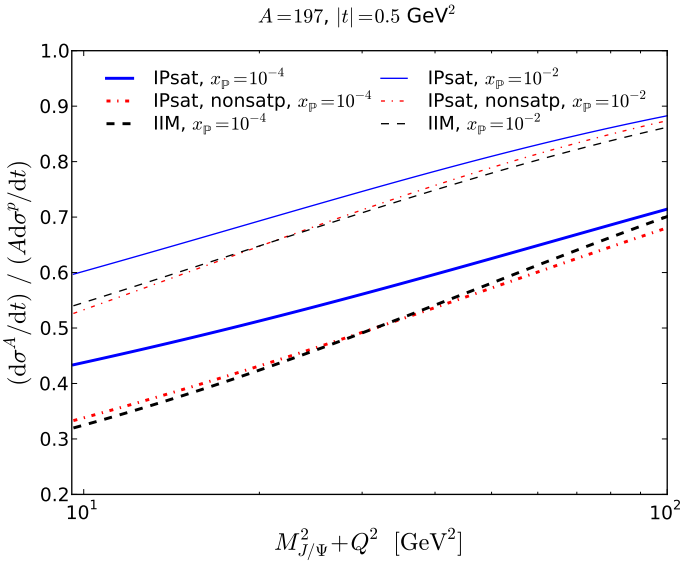

(a) Boosted-Gaussian

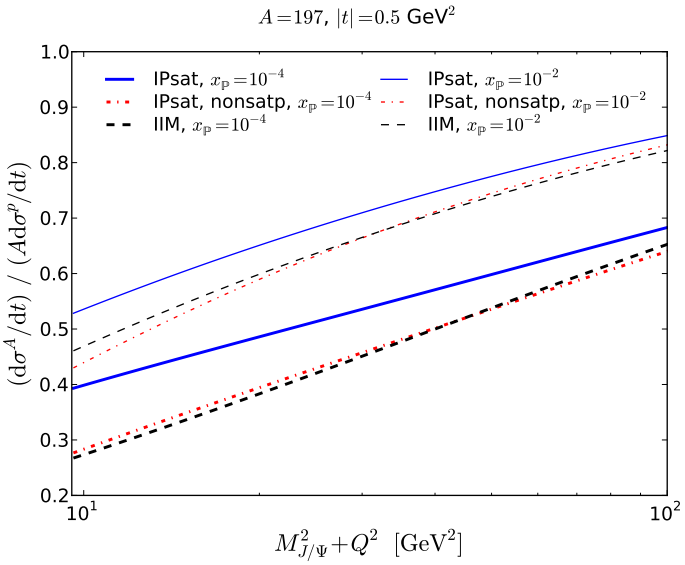

(b) Gaus-LC

Figure 12. The nuclear transparency ratio of cross sections as a function of Q^2 for IPsat and IIM models at $x_{\mathbb{P}} = 10^{-2}$ (upper curves) and 10^{-4} (lower curves) using different parametrizations for the wave function overlap.

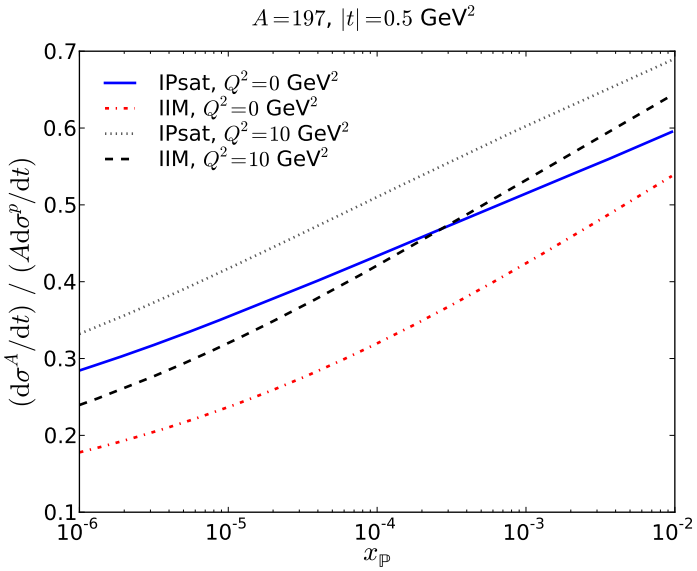

Figure 13. The nuclear transparency ratio of cross sections as a function of $x_{\mathbb{P}}$ using the IIM and IPsat parametrizations.

The effect of different vector meson wave functions, discussed in Sec. 2.3, is also studied. In Fig. 12 we have plotted the Q^2 dependence of the nuclear suppression factor using both boosted-Gaussian and Gaus-LC parametrizations for the wave function overlap. The results differ, as Gaus-LC puts more weight on large dipole sizes (see e.g. Ref. [5]), which leads to stronger suppression.

For comparison we also consider an unphysical model in which the dipole-proton cross section $\mathcal{N}$ does not saturate, but we generalize it to dipole-nucleus scattering in the same way than with the IPsat model. This model is labeled as "IPsat, nonsat p" and corresponds to including unitarity effects at the nucleus level but not for a single nucleon. As can be seen from Fig. 12, the nuclear suppression in this scenario is significantly larger than the one for the correct IPsat parametrization. This shows that the nuclear suppression is sensitive to saturation effects already at the proton level.

In addition, we also computed the nuclear suppression as a function of $x_{\mathbb{P}}$, shown in Fig. 13. From these numerical calculations one can clearly see that the IIM parametrization has much larger nuclear suppression in incoherent diffraction than the IPsat model. Recall that both IPsat and IIM models describe the HERA data very accurately, as was discussed in Sec. 2.4 and shown in Fig. 8.

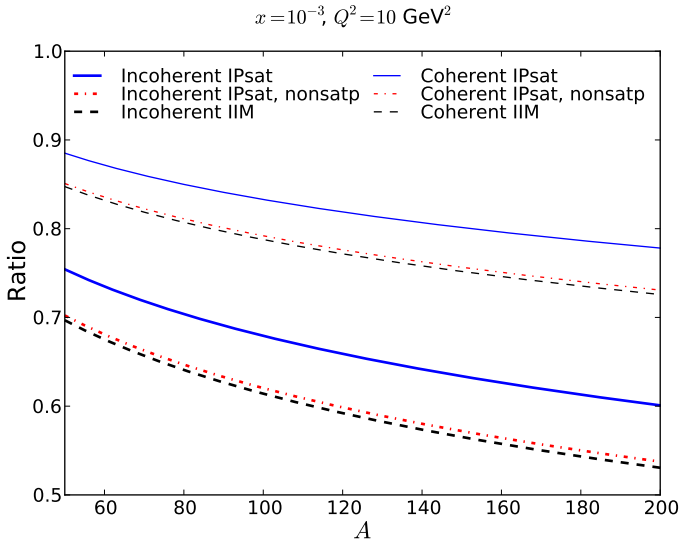

Figure 14. Mass number A dependence of the ratio of coherent (at $t = 0$) and incoherent (at $t = -0.5$ GeV^2, but in our approximation this is t-independent) cross sections to the corresponding ones for a proton normalized with A^2 and A, respectively.

To understand where this difference comes from notice that the elastic dipole-proton cross section $\sigma^{\mathrm{el}}_{q\bar{q}} \sim B_p \mathcal{N}^2$. As both of these models work with the diffractive HERA data, the elastic cross sections are the same. But as B_p is larger in the IIM model, $\mathcal{N}$ must be smaller. Moreover, the nuclear suppression factor, Eq. (3.23), depends on the total cross section $B_p \mathcal{N} \sim \sigma^{\mathrm{el}}_{q\bar{q}}/\mathcal{N}$. Thus the suppression is clearly larger in the IIM model.

The relative similarity of the nuclear suppression in the coherent and incoherent cross sections is demonstrated in Fig. 14. To see that we have plotted the A dependence of the ratios

$$\frac{\mathrm{d}\sigma^A_{\mathrm{incoh}}/\mathrm{d}t}{A\mathrm{d}\sigma^p/\mathrm{d}t} \quad \text{and} \tag{3.27}$$

$$\left.\frac{\mathrm{d}\sigma^A_{\mathrm{coh}}/\mathrm{d}t}{A^2\mathrm{d}\sigma^p/\mathrm{d}t}\right|_{t=0}. \tag{3.28}$$

Notice that these ratios are normalized by different powers of A. In our approximation the ratio (3.27) does not depend on t, as the t-dependence is factorized in Eqs. (3.16) and (2.30).

4 Conclusions

In this work we derived an analytical approximation, Eq. (3.22), for a vector meson production in incoherent diffractive γ^*-nucleus scattering and studied the saturation effects on dipole-nucleus scattering. We used our results to compute the realistic first estimates for the absolute cross section and nuclear suppression factor which could be measured in future nuclear DIS experiments.

As a result we saw that the nuclear suppression factor is large and must be taken into account when considering future nuclear DIS experiments. We also found that the suppression is model-dependent, and it is much larger in the IIM model than in the IPsat model. The main results of this work are equation (3.22) and figures 11, 12 and 13.

We also noticed that different models for the virtual photon wave function lead to somewhat different nuclear suppression factors, as shown in Fig. 12. Current experimental data does not allow us to determine which model for the dipole-proton scattering amplitude and for the virtual photon wave function is the best one.

Although a similar expression as Eq. (3.22) for incoherent vector meson production was derived before this work in Ref. [19], the unitarity effects are not very well known. Our work (figure 11) clearly shows that the small dipole approximation, the IPnonsat model that is still used, clearly overestimates the dipole-nucleus cross section and it should not be used when one considers e.g. future nuclear DIS experiments.

In our work we made several simplifying assumptions which may affect the cross section or nuclear suppression factor. Namely we approximated that we can factorize the impact parameter dependence and that the dipole scatters off the nucleons inside the nucleus independently. We also neglected possible nucleon-nucleon correlations. These approximations allowed us to derive analytically a realistic estimate for the incoherent dipole-nucleus cross section which is still easy to evaluate numerically. Including these effects in a physically correct manner was beyond the scope of this research and is left for future work.

References

[1] T. Lappi and H. Mäntysaari, "Incoherent diffractive J/Ψ production in high-energy nuclear deep-inelastic scattering," *Phys. Rev.* **C83** (2011) 065202, arXiv:1011.1988 [hep-ph].

[2] A. Deshpande, R. Milner, R. Venugopalan, and W. Vogelsang, "Study of the fundamental structure of matter with an electron ion collider," *Ann. Rev. Nucl. Part. Sci.* **55** (2005) 165–228, arXiv:hep-ph/0506148.

[3] J. B. Dainton, M. Klein, P. Newman, E. Perez, and F. Willeke, "Deep inelastic electron nucleon scattering at the LHC," *JINST* **1** (2006) P10001, arXiv:hep-ex/0603016.

[4] E. Predazzi and V. Barone, *High-Energy Particle Diffraction*. Springer, 1 ed., 2002. ISBN 978-3540421078.

[5] H. Kowalski, L. Motyka, and G. Watt, "Exclusive diffractive processes at HERA within the dipole picture," *Phys. Rev.* **D74** (2006) 074016, arXiv:hep-ph/0606272.

[6] H. Kowalski and D. Teaney, "Impact parameter dipole saturation model," *Phys. Rev.* **D68** (2003) no. 11, , arXiv:hep-ph/0304189v3.

[7] E. Iancu and R. Venugopalan, "The Color glass condensate and high-energy scattering in QCD," arXiv:hep-ph/0303204 [hep-ph]. To be published in QGP3, Eds. R.C. Hwa and X.N.Wang, World Scientific.

[8] Y. V. Kovchegov, "Small-x F_2 structure function of a nucleus including multiple pomeron exchanges," *Phys.Rev.* **D60** (1999) 034008, arXiv:hep-ph/9901281 [hep-ph].

[9] I. Balitsky, "Operator expansion for high-energy scattering," *Nucl. Phys.* **B463** (1996) 99–160, arXiv:hep-ph/9509348.

[10] C. Marquet, "A unified description of diffractive deep inelastic scattering with saturation," *Phys. Rev.* **D76** (2007) 094017, arXiv:0706.2682 [hep-ph].

[11] G. Watt and H. Kowalski, "Impact parameter dependent colour glass condensate dipole model," *Phys. Rev.* **D78** (2008) 014016, arXiv:0712.2670 [hep-ph].

[12] **ZEUS** Collaboration, S. Chekanov *et al.*, "Exclusive electroproduction of J/Ψ mesons at HERA," *Nucl. Phys.* **B695** (2004) 3–37, arXiv:hep-ex/0404008.

[13] **H1** Collaboration, A. Aktas *et al.*, "Elastic J/Ψ production at HERA," *Eur. Phys. J.* **C46** (2006) 585–603, arXiv:hep-ex/0510016.

[14] A. G. Shuvaev, K. J. Golec-Biernat, A. D. Martin, and M. G. Ryskin, "Off-diagonal distributions fixed by diagonal partons at small x and ξ," *Phys. Rev.* **D60** (1999) 014015, arXiv:hep-ph/9902410.

[15] F. Halzen and A. D. Martin, *Quarks & Leptons*. Wiley, 1984. ISBN 978-0471887416.

[16] **H1** Collaboration, S. Aid *et al.*, "Elastic Electroproduction of ρ and J/Ψ Mesons at large Q^2 at HERA," *Nucl.Phys.* **B468** (1996) 3–36, arXiv:hep-ex/9602007 [hep-ex].

[17] R. D. Woods and D. S. Saxon, "Diffuse surface optical model for nucleon-nuclei scattering," *Phys. Rev.* **95** (1954) no. 2, 577–578.

[18] A. Caldwell and H. Kowalski, "Investigating the gluonic structure of nuclei via J/Ψ scattering," *Phys. Rev.* **C81** (2010) 025203, arXiv:0909.1254.

[19] B. Z. Kopeliovich, J. Nemchik, A. Schafer, and A. V. Tarasov, "Color transparency versus quantum coherence in electroproduction of vector mesons off nuclei," *Phys. Rev.* **C65** (2002) 035201, arXiv:hep-ph/0107227.